Effect of Deposition Geometry on Multiphase Flow of Wells Producing Asphaltenic and Waxy Oil Mixtures

Edgar Ramirez-Jaramillo,*,† Jose M. del Rio,† Octavio Manero,‡ and Carlos Lira-Galeana†

Mexican Inst. of Petroleum, Eje Central Lazaro Cardenas 152, San Bartolo Atepehuacan, Mexico 07730, D.F., Mexico, and Materials Research Institute, National Autonomous University of Mexico, Ciudad Universitaria, 04510, Mexico, D.F., Mexico

Heavy organic deposition (asphaltenes, waxes, hydrates, etc.) on the wall of oil pipelines is often regarded as a serious problem due to technical and economic implications. Because the asphaltene deposition causes an effective reduction of the cross section of the pipes, it is important to study the effect of this reduction on the most important hydrodynamic parameters of a well, such as pressure drops, flow regimes, and inflow performance behavior, just to mention a few. To address the role of reductions to the flow of hydrocarbons in vertical pipe systems, we present a compositional flow model that accounts for reductions to the flow of a produced hydrocarbon mixture. In this work, we study producing wells ("A" and "B") located in southeast of Mexico. In the case of well A, we show the results of an asphaltene deposition simulation and the total pressure drop as a function of time along the pipeline, while for well B, we show the results obtained for the total pressure drop as a function of the different artificial reductions along the well.

1. Introduction

Sudden reductions/expansions to the cross section of pipes transporting hydrocarbons are often encountered in industry. Examples include the use of choke-valves in different sections of an oil well or the occurrence of heavy depositions (asphaltenes, wax, hydrates, scales) that threaten flow assurance. These reductions lead to significant alterations to various hydrodynamic parameters of a well, such as pressure drops, flow regimes, and inflow performance behavior, just to mention a few. For these systems, multiphase flows can be present in pipeline networks often involving sudden area changes in the form of chokes, valves, elbows, orifices, or heavy organic deposits which agglomerate and adhere to the pipeline walls. For efficient description of petroleum production processes, it is important to understand the effect that such restrictions have on different parameters related to the flow, such as temperature/pressure drops, the void fraction, and the estimated flow regimes for a given well. When changes to the effective cross section of a pipe in the form of restrictions arise, the effect of such changes on the global performance of the transport process must be considered.

When a liquid mixture flows past a restriction, it is known that its velocity increases and its pressure decreases. The essentially empirical correlations for pressure drop through restrictions developed to date are focused to predict the dependence of pressure drop on velocity throughout the restriction. In petroleum applications, the existing correlations for oil−gas−water systems have limitations in describing the conditions which determine the limits among the critical and subcritical flows in multiphase mixtures in chokes. Therefore it is important to address the computation of pressure drop and the entire performance of pipes undergoing flow restrictions of virtually any form, using a set of recently developed tools for describing the hydrodynamic behavior of complex systems.

2. Literature Review

Over the past 25 years, a significant number of papers dealing with two-phase (liquid−gas) flows have been reported in the literature. Most of these works are devoted to experimental studies on flows through constant-section tubes. The goal of these works is to obtain empirical correlations for flow parameters such as pressure drop, vapor void fraction, or heat transfer. Models for liquid−gas flows undergoing changes in the effective cross section have received much less attention. For instance, Neusen,[1] Maneely,[2] Brown,[3] and Fiedler[4] investigated the flow of water through convergent/divergent nozzles. Vorgin[5] studied the flow of air−water mixtures throughout nozzles. Hessen and Peck[6] performed experiments with flowing carbon dioxide throughout horizontal orifices and nozzles.

Petrick[7] reported a study on the effect of a sequential expansion-contraction process in a pipe transporting a water−air mixture flowing upward a vertical (open) channel. The weight fraction of air was in all cases above 0.0045. He also monitored the changes in flow regimes using a camera. He concluded that the transition following a sudden contraction/expansion is a function of the gas fraction, total mass flow, and area ratio. He also reported that the transition zone following a contraction was not as pronounced as in the case of an expansion.

Straub and Silverman[8] reported measurements of pressure drop for air−water flows throughout sudden contraction/expansions in a horizontal pipe. Using their model, these authors were unable to correlate the measured data. Janssen and Kervinen[9] measured the change in pressure that water flows undergo through expansions from 0.0508 to 0.0889 m (2−3.5 in.) and 0.1143 to 0.1397 m (4.5−5.5 in.) expanders and contractions from 0.0889, 0.1143, and 0.1397 to 0.0508 m (3.5, 4.5, and 5.5 to 2 in). The tests were performed on vertical pipes and flows in the upward direction. The measured pressure drops were correlated via the Romie equation. The error in calculated results was within 25% of the measured data.

Aloui and Souhar[10] reported an experimental study on bubble flows throughout a sudden, horizontal flat expansion. For a quasi-symmetric bubble flow, both the pressure and volume fraction increased downstream.

---

* To whom correspondence should be addressed. Tel.: +52 55 9175-6507. E-mail address: eramirez@imp.mx.
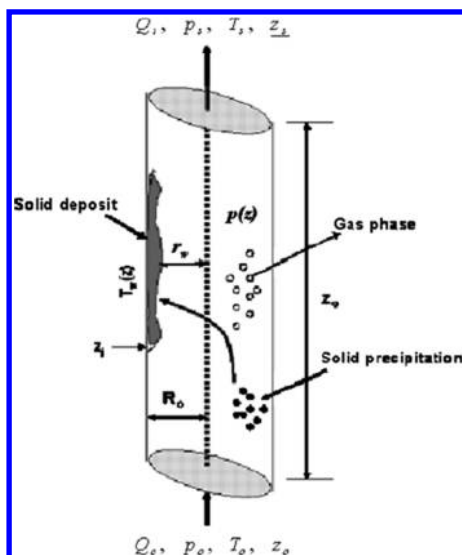† Mexican Inst. of Petroleum.
‡ National Autonomous University of Mexico.

Figure 1. Solid deposition in a model pipe.

Ahmed[11] developed an analytical formulation of pressure drop for a two-phase flow throughout a sudden expansion. His model takes into account the change in the volume fraction during the expansion, the shear stress at the wall, the pressure difference between the flow upstream of the contraction and the fully developed flow region downstream of the expansion. Chen et al.[12] performed experimental studies to address the pressure changes and flow regimes subjected to the influence of sudden contractions. Water−air mixtures were used, flowing along rectangular ducts. The flow rates varied between 100 and 700 kg/m^2 with gas weight fractions in the range of 0.001−0.8. In general, they observed that the pressure at the contraction increased both with the gas amount and mass flux.

In this work, we analyze two real wells. Well "A" shows results from the proposed model on the calculation of the asphaltene deposit profile along the pipe and how the position and shape of the deposit affect the dynamic axial pressure gradient. Well "B" analyzes the effect of changes in the geometrical configuration of the transverse area at several axial positions. The objective of this analysis is to establish the changes of the dynamic axial pressure gradient as a function of the effective diameter, position, and shape of the artificial deposit along the pipe. As the pressure gradient changes, the pressure near the surface diminishes and hence the flow rate changes. This study aims to provide better understanding of the relationship between well production and shape, dimension, and position of restrictions along the production well.

3. Proposed Model

The multiphase flow model proposed in this work has been described in the work of Ramírez-Jaramillo et al.[13] In this work, we outline the most important details. Figure 1 presents the flow system schematically. A pipe region of dimensions r and z and length L contains a flowing liquid with initial composition. The fluid is a hydrocarbon mixture of n-components, and thus, the mole fractions of the different phases (liquid, solid, gas, and water, if present) are functions of pressure and temperature at a given pipe location. The pipe has an inner radius R_o and transports a multicomponent hydrocarbon mixture that enters the bottom of the pipe at an initial pressure p_o, temperature T_o, and volumetric flow rate Q_o. The outer pipe temperature and the fluid pressure change along the length of the pipe, and

consequently, the fluid is cooled and expanded as it follows its upward motion. The forced-convection heat-transfer process induces a change in the liquid temperature. Due to the fact that the goal of this model is the study of solid organic deposition (asphaltenes and waxes), we take into account that, under turbulent flow, the important region for this analysis is the laminar sublayer. Hence, the flow regions in this case include a turbulent core, a transition zone, and the laminar sublayer. In the turbulent core, heat transport is fast and the radial variation of the temperature profile is negligible. In the region next to the wall, heat conduction across the laminar sublayer is assumed, and hence, a more pronounced temperature drop occurs. In the transition zone, heat conduction and turbulent heat transport are present.

The calculation procedure used to obtain the pressure drop along the vertical pipe considers the combined effect of the energy lost friction, the change in potential energy, and the change in kinetic energy. This energy balance, which is basic to all pressure-drop calculations, can be generally written as

$$\left(\frac{dP}{dz}\right)_{Tot} = \left(\frac{dP}{dz}\right)_{el} + \left(\frac{dP}{dz}\right)_{fr} + \left(\frac{dP}{dz}\right)_{acc} \quad (1)$$

The total pressure gradient includes the contributions of acceleration (ac), elevation (el), and friction (fr). A characteristic property of multiphase flow is the presence of flow regimes representing the distribution of phases inside the pipe. Various flow patterns are found depending on pressure and temperature conditions, flow rate, pipe diameter, and fluid properties. This complexity is due to changes in composition, flow rate, physical properties of each phase resulting from the pressure drop, and heat transfer with the surroundings. In most analyses, four flow regimes are considered (bubble flow, slug flow, transition flow, and mist flow) which may occur in a vertical pipe. These flow regimes affect the pressure gradient which itself affects the temperature, heat transfer, and deposition processes. Therefore, the flow regime is assumed to affect the deposition process indirectly. Nevertheless, in every flow regime, it is always possible to find a narrow laminar layer (the viscous or heat sublayer) of fluid next to the wall. Within this layer, laminar flow allows molecular diffusion of asphaltene aggregates in the radial direction. In the core, on the other hand, the temperature profile is assumed flat, and therefore, the flow regime affects the deposition process through the pressure gradient, which itself is a function of the flow regime.

On the basis of its ability to match measured pressure drops in producing wells, the compositional, equation of state (EOS) based model by Ramirez-Jaramillo et al.[13] uses the pressure drop correlations developed by Mukherjee and Brill[14] and Dun and Ros.[15] Details of these correlations are presented in Appendix A. Study wells A and B analyze the cases of asphaltene deposition and liquid−vapor equilibrium without deposition, respectively.

The computational procedure used in this work involves the calculation of the pressure and temperature profiles in a well, where the multiphase pressure-drop correlation is used together with the Peng and Robinson[16] and SAFT-VR[17] (self-associating fluid theory) equations of state for computing the gas−liquid phase equilibrium and asphaltene deposition. The corresponding iterative procedure for the whole calculation is depicted in Figure 2. After discretization of the pipe in a number of segments along the axial direction, calculations determine the temperature and pressure at the extreme of each segment. The model should satisfy primarily the heat balance together with the phase equilibrium relations, and in addition, it should estimate a value
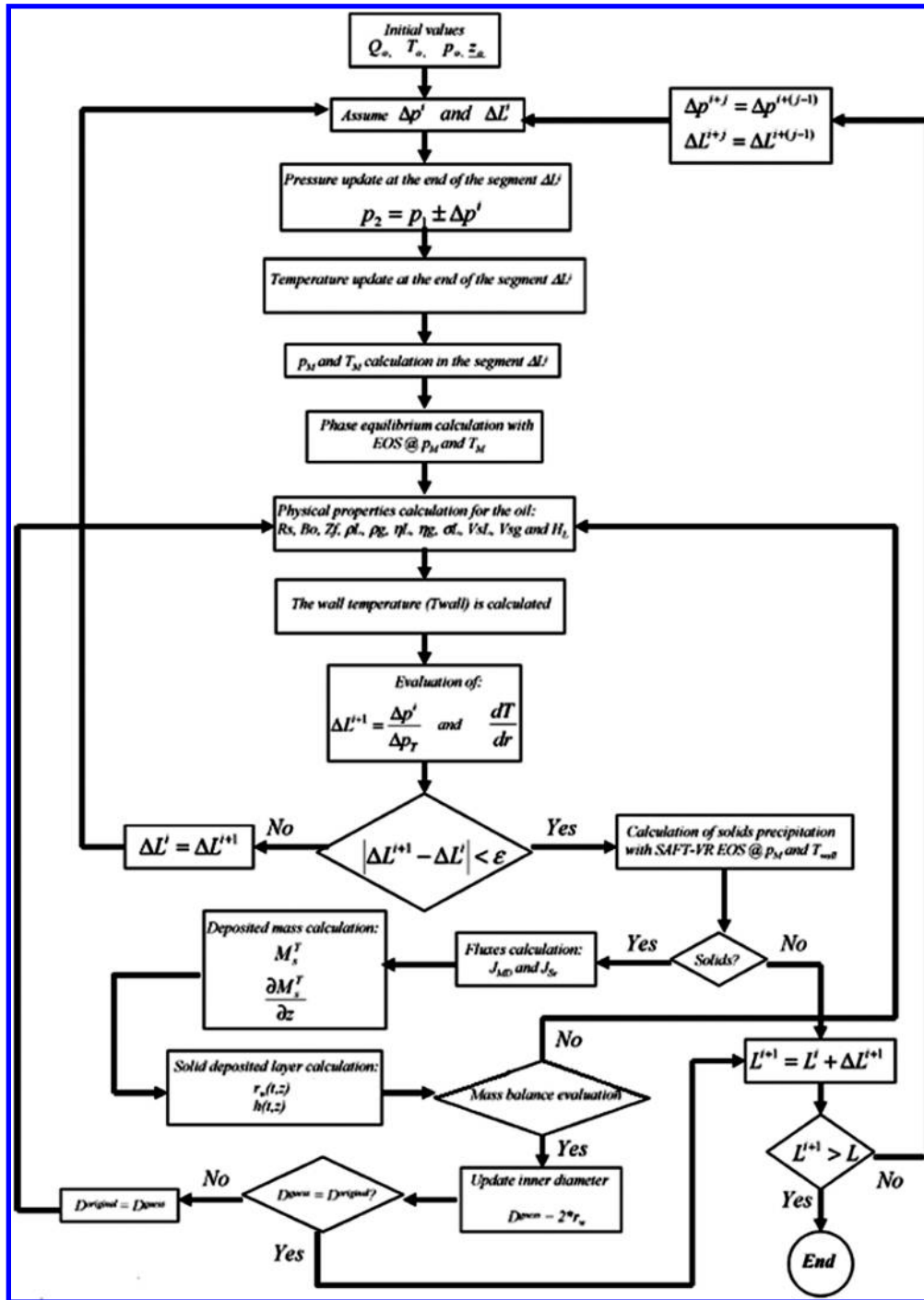
Figure 2. Computational procedures.

of the segment pressure that must converge to the predetermined pressure estimate at each segment. The following steps complete the algorithm:

(1) At a given pipe length where the pressure is known (p_1, L_1), a pressure drop is assumed for the next segment length (Δp^i and ΔL^i), in addition to the temperature of the reference segment (T_1) and the height of the controlled volume.

(2) With these initial values of length and pressure, the pressure is updated at the end of the segment ($p_2 = p_1 \pm \Delta p^i$), where $\pm$ indicates the calculation direction.

(3) With p_2, the PVT properties are determined to implement the Romero-Juarez[18] correlation for the fluid temperature

(T_2), which is given by the following relations:

$$T(z) = T_{wf} - G_e(A(1 - e^{-z/A}) - z) \tag{2}$$

where

$$A = \frac{86400 W_f C_f (K_e + DUF_T)}{2\pi DK_e U} \tag{3}$$

In eqs 2 and 3, D is the pipe diameter, U is the global heat transfer coefficient, T_{wf} is the bottom well flowing temperature, z is the length, W_f is the mass flow rate, and C_f is the specific heat of the fluid. K_e and G_e are

Table 1. Mechanical Configuration of Well A

# pipe section	D_{in}/m	ΔL/m	roughness/m	inclination angle
		TR		
1	0.06985	1275.83404	0.0000508	53.9408
2	0.06985	127.46710	0.0000508	48.3167
3	0.06985	116.23980	0.0000254	54.8700
4	0.06985	179.95001	0.0000254	64.8114
5	0.06985	329.19471	0.0000254	74.8583
6	0.06985	3321.62891	0.0000254	89.3963

Table 2. Composition of the Reservoir Fluid of Well A

component	molecular weight	% mol
CO_2	44.01	1.05
H_2S	34.08	0.02
N_2	28.01	0.71
C1	16.04	37.87
C2	30.07	11.48
C3	44.10	6.55
i-C4	58.12	0.91
n-C4	58.12	2.96
i-C5	72.15	1.39
n-C5	72.15	2.15
C6	85.00	2.64
methyl-cyclo-C5	84.16	0.56
benzene	78.11	0.62
cyclo-C6	82.15	0.77
C7	99.00	1.86
methyl-cyclo-C6	98.19	0.68
toluene	92.14	0.29
C8	113.00	2.83
ethyl-benzene	106.17	0.23
M- and P-xylene	106.17	0.23
O-xylene	106.17	0.08
C9	128.30	2.55
C10	134.00	2.66
C11	147.00	2.04
C12	161.00	1.48
C13	175.00	1.20
C14	190.00	0.96
C15+	206.00	0.77
C16	222.00	0.59
C17	237.00	0.42
C18	251.00	0.33
C19	263.00	0.30
C20	275.00	0.25
C21	291.00	0.20
C22	305.00	0.16
C23	318.00	0.11
C24	331.00	0.10
C25	345.00	0.06
C26	359.00	0.06
C27	374.00	0.05
C28	388.00	0.03
C29	402.00	0.02
C30+	580.00	9.79

the geothermal conductivity and gradient of the fluid, respectively. F_t is a time-dependent function valid for times (t) less than 400 days:

$$\log F(t) = 0.31333 \log Y - 0.06(\log Y)^2 + 0.006666(\log Y)^3 \tag{4}$$

where

$$Y = \frac{552t}{D^2} \tag{5}$$

Otherwise, if $t \geq 400$ days, then $F_T = 1$.

(4) Once the pressure and temperature at the extremes are known, the mean values of pressure and temperature of the segment are determined (p_M and T_M).

Table 3. SARA Analysis of the Stock-Tank Oil of Well A

% saturates	46.89
% aromatics	33.07
% resins	17.30
% asphaltens	2.72

(5) According to these mean values, the *PVT* properties of the mixture are determined (Rs, Bo, Z_f, ρ_L, ρ_g, η_L, η_g, σ_L, V_{sL}, and V_{sg}). Thereafter, the total pressure drop in the segment is calculated according to eq 1, in addition to the Reynolds number (Re), liquid holdup (H_L), the mixture density, and estimation of the flow patterns.

(6) The wall temperature (T_{wall}) is calculated as follows:

$$T_{wall} = T_{fluid} - \frac{Q}{h_{in}A} \tag{6}$$

where T_{fluid} is the mean temperature in the core, Q is the heat flux, A is the inner surface, and h_{in} is the heat transfer coefficient which changes according to the type of flow:

$$h_{in} = 0.026\frac{k_b}{D}\left(\frac{D\rho_m v_s}{\eta_b}\right)^{0.8}\left(\frac{C_p\eta}{k_b}\right)^{1/3}\left(\frac{\eta_b}{\eta_o}\right)^{0.14} \quad Re > 20\,000 \tag{7}$$

$$h_{in} = 0.026\frac{k_b}{D}\left(\frac{D\rho_m v_s}{\eta_b}\right)^{0.8}\left(\frac{C_p\eta}{k_b}\right)^{1/3}\left(\frac{\eta_b}{\eta_o}\right)^{0.14} \quad Re < 20\,000 \tag{8}$$

D and L are the pipe diameter and length, respectively, Pr is the Prandtl number, C_p is the heat capacity of the mixture, η_b and k_b are the viscosity and thermal conductivity of the mixture.
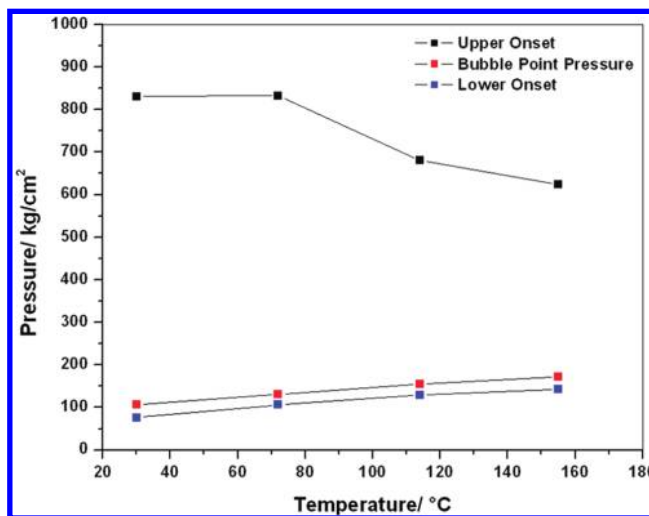

Figure 3. Asphaltene precipitation envelope for well A.

Table 4. Production Data of Well A

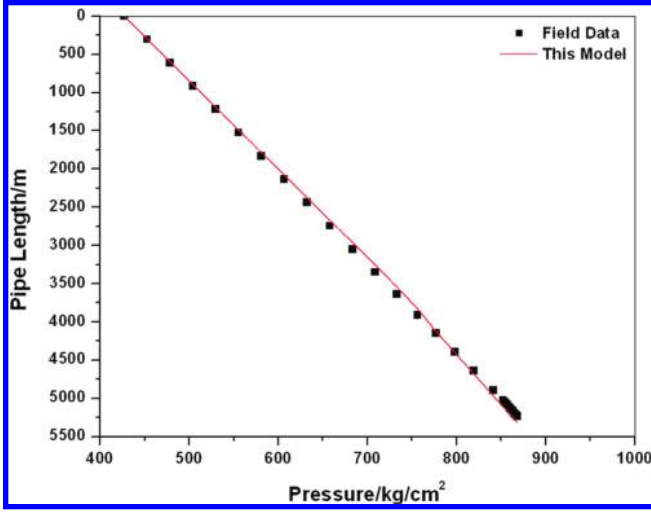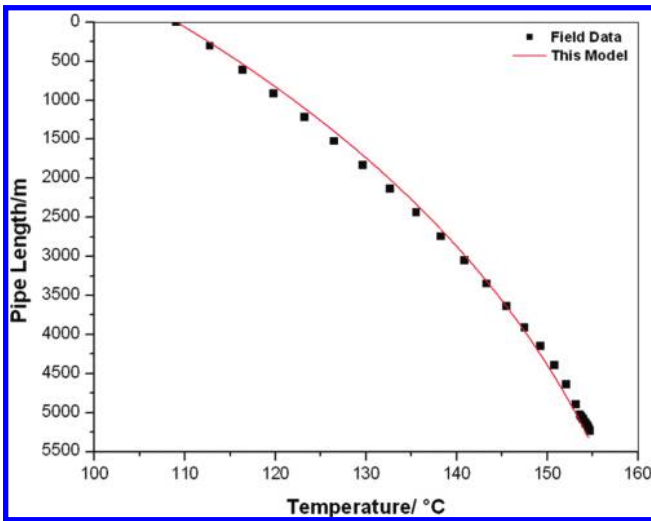| parameter	value
P_{wf}/kg/cm^2	868.3
P_{wh}/kg/cm^2	427.3
T_{wf}/°C	154.7
T_{wh}/°C	109.1
°API	30.2
GOR/m^3/m^3	110
% H_2O	0
P_b at T_{wf}/kg/cm^2	172.9
Q_o/BPD	4964.5
Q_g/mmscd	3.1
U/Btu/h·ft^2·°F	4.5

Figure 4. Matching of the pressure gradient of well A.

Figure 5. Matching of the temperature gradient of well A.

Table 5. Mechanical Configuration of Well B

	no. pipe segment	$D_{in}t$/m	ΔL/m	roughness/m	inclination angle
TR	1	0.1086	380.0856	0.00001524	73.000
	2	0.1086	20.1168	0.00001524	71.146
TP	3	0.0582	123.7488	0.00001524	84.282
	4	0.0760	870.0516	0.00001524	62.511
	5	0.0760	369.9967	0.00001524	59.550
	6	0.0760	59.9846	0.00001524	71.075
	7	0.1005	1820.1711	0.00001524	56.443
	8	0.0968	0.9997	0.00001524	90.000
	9	0.1005	126.4402	0.00001524	90.000

(7) The length increase is evaluated according to $\Delta L^{i+1} = \Delta p^i / \Delta P_t$ for the segment considered. If ΔL^i and ΔL^{i+1} are equal, the procedure continues to step 8; otherwise, step 2 is repeated.

(8) If ΔL^{i+1} are equal to or larger than the total pipe length, then the calculation concludes; otherwise, the calculation proceeds with the next pipe segment. For the case of solids deposition, the following steps are applied to the computation scheme.

(9) The radial temperature gradient dT/dr is calculated using the approximation $dT/dr \approx \Delta T/\Delta r$, where $\Delta T = T_{wall} - T_{fluid}$ and Δr is the width of the boundary layer.

(10) The wall temperature and mean segment pressure T_{wall} and p_M are used to calculate the phase equilibrium, which
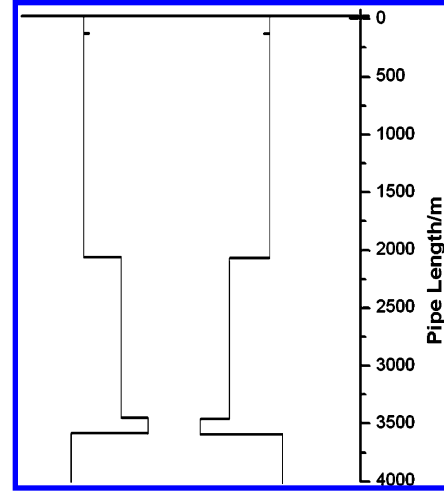

Figure 6. Mechanical configuration of well B.

renders the properties and amounts of the fluid phases (liquid and gas) and solid phase (asphaltenes). In the case of the appearance of solid fractions, the procedure continues to step 11; otherwise, it continues to step 19.

(11) The mass flux of the solid-phase components[19] is calculated according to Fick's law, and the solids amount removed by the shear stress, as suggested by Kern and Seaton,[20] is calculated, respectively:

$$J_{MD} = \sum_{i=1}^{n} J_{MD}^i = -D\rho_m \sum_{i=1}^{n} \left[-T \frac{\partial w_{si}}{\partial T} + (1 - w_{si}) \frac{T}{\rho_m} \frac{\partial \rho_m}{\partial T} \right] \frac{1}{T} \frac{\partial T}{\partial r} \quad (9)$$

and

$$J_{sr} = A_1 \tau_P M_S^t(t - dt, z) \exp\left(-\frac{B_1}{T} \right) \quad (10)$$

In eqs 9 and 10, w_{si} is the solid fraction of the i component in the solid phase; D is the diffusion coefficient; T is the average temperature in the interval; ρ_m is the mixture density; τ_p is the shear stress at the wall; $M_S^T(t - dt, z)$ is the solid mass deposited at a given time (t); constants A_1 and B_1 depend on the oil composition.

(12) The total mass deposited on the pipe inner wall for a given time at a distance z from the entrance section is calculated for each component in the solid phase according to[19]

$$\frac{\partial M_S^i(t + \Delta t, z)}{\partial z} = \frac{\partial M_S^i(t, z)}{\partial z} + 2\pi \int_t^{t+\Delta t} r_w(t, z)(J_{MD}^i - J_{SR}) \, dt \quad (11)$$

where $r_w (t = 0, z) = Ro$ is the effective inner pipe radius.

(13) The effective pipe radius $r_w (t, z)$ and the width of the deposited layer $h(t, z)$ are updated according to

$$r_w(t, z) = \left(R_o^2 - \frac{1}{\pi \rho_S} \frac{\partial M_S}{\partial z} \right) \quad (12)$$

and

$$h(t, z) = R_o - r_w(t, z) \quad (13)$$

Table 6. Composition of the Reservoir Fluid of Well B

component	MW	API	T_b/°C	T_c/°C	P_c/kg/cm^2	V_c/bbl/bl-mol	ω_i	z_i
H$_2$O	18.015000	10.063000	100.000000	374.200000	225.553000	0.158100	0.348000	0.42030000
N$_2$	28.013000	43.600000	−195.800000	−146.900000	34.613000	0.257100	0.045000	0.00096625
CO$_2$	44.010000	39.600000	−78.480000	31.040000	75.271000	0.268200	0.231000	0.00296260
H$_2$S	34.079000	47.600000	−60.340000	100.400000	91.854000	0.278700	0.100000	0.01550000
methane	16.043000	340.167000	−161.490000	−82.600000	46.908000	0.282400	0.010400	0.26750000
ethane	30.070000	265.526000	−88.630000	32.300000	49.802000	0.422200	0.098600	0.06812260
propane	44.097000	147.208000	−42.070000	96.670000	43.334000	0.579200	0.152900	0.04290000
i-butane	58.124000	119.788000	−11.730000	134.980000	37.196000	0.750300	0.177200	0.00823920
butane	58.124000	110.629000	−0.500000	152.000000	38.746000	0.727500	0.201300	0.02140000
22PR	72.151000	105.638000	9.500000	160.590000	32.619000	0.864500	0.197000	0.00026429
i-pentane	72.151000	95.727000	27.850000	187.240000	34.479000	0.873000	0.229000	0.00801260
pentane	72.151000	92.747000	36.074000	196.500000	34.355000	0.867300	0.250600	0.01120000
CP	70.135000	57.025000	49.260000	238.500000	45.968000	0.741800	0.195800	0.00073182
hexane	86.178000	81.602000	68.740000	234.200000	30.274000	1.055600	0.294300	0.00001026
NBP-73	86.722000	66.397000	73.611000	252.532000	33.654000	1.015500	0.252820	0.01330000
NBP-87	93.216000	63.881000	87.180000	267.482000	32.033000	1.086000	0.273710	0.01210000
NBP-106	103.199000	60.547000	106.272000	288.281000	29.970000	1.189300	0.303390	0.00998670
NBP-126	114.292000	57.260000	126.443000	309.948000	28.012000	1.304000	0.335150	0.00909060
NBP-144	124.723000	54.478000	144.646000	329.220000	26.407000	1.412600	0.364280	0.00844980
NBP-164	136.950000	51.611000	164.577000	350.007000	24.797000	1.537200	0.396830	0.00621960
NBP-183	149.497000	49.028000	183.640000	369.579000	23.382000	1.662000	0.428760	0.00655180
NBP-203	163.158000	46.548000	202.994000	389.145000	22.057000	1.794300	0.462110	0.00547660
NBP-222	178.029000	44.167000	222.620000	408.678000	20.814000	1.934000	0.497000	0.00554500
NBP-242	193.722000	41.943000	241.933000	427.610000	19.683000	2.076800	0.532510	0.00561350
NBP-261	210.612000	39.815000	261.363000	446.385000	18.627000	2.225400	0.569500	0.00515520
NBP-281	228.787000	37.771000	280.970000	465.071000	17.639000	2.380100	0.608180	0.00495300
NBP-300	247.838000	35.840000	300.366000	483.322000	16.732000	2.537300	0.647850	0.00518250
NBP-319	267.380000	34.035000	319.333000	500.962000	15.908000	2.694600	0.688030	0.00414590
NBP-339	288.498000	32.231000	339.137000	519.185000	15.108000	2.862000	0.731470	0.00342150
NBP-358	309.509000	30.535000	358.567000	536.890000	14.379000	3.028900	0.775570	0.00315260
NBP-378	330.200000	28.905000	378.020000	554.466000	13.699000	3.198100	0.821210	0.00286940
NBP-397	351.497000	27.337000	397.496000	571.930000	13.065000	3.369000	0.868350	0.00268780
NBP-416	378.678000	25.844000	416.762000	589.094000	12.479000	3.539100	0.916360	0.00236020
NBP-444	417.561000	23.768000	444.812000	613.921000	11.692000	3.787900	0.988570	0.00354300
NBP-481	467.902000	21.190000	481.790000	646.427000	10.760000	4.116000	1.087490	0.00284490
NBP-519	519.508000	18.721000	519.631000	679.525000	9.909000	4.450600	1.192120	0.00240790
NBP-555	570.362000	16.522000	555.495000	710.817000	9.182000	4.765700	1.293110	0.00237290
NBP-591	626.096000	14.424000	591.755000	742.448000	8.511000	5.082100	1.395300	0.00134020
NBP-628	689.882000	12.412000	628.539000	774.596000	7.884000	5.401200	1.496780	0.00075499
NBP-667	768.393000	10.405000	667.336000	808.633000	7.271000	5.736100	1.598250	0.00067094
NBP-713	886.442000	8.151000	713.609000	849.505000	6.592000	6.133400	1.705840	0.00047430
NBP-767	1063.087000	5.710000	767.226000	897.406000	5.859000	6.589600	1.799290	0.00041747
NBP-875	1487.265000	1.264000	875.284000	996.671000	5.181000	6.958000	2.116740	0.00079668

Table 7. Production Data of Well B

parameter	value
P_{wf}/kg/cm^2	233.6
P_{wh}/kg/cm^2	64
T_{wf}/°C	157.6
T_{wh}/°C	97
°API	34.1
GOR/ft^3/bbl	1756
% H$_2$O	18.6
P_b @ T_{wf}/kg/cm^2	220
Q_t/BPD	4000
Q_o/BPD	3254
U/Btu/h·ft^2·°F	4.5

(14) The deposited solid mass for each component along the length of the pipe at time $t + \Delta t$ is calculated according to

$$M_S^i(t + \Delta t) = M_S^i(t) + \int_0^L \frac{\partial M_S^i(t + \Delta t, z)}{\partial z} \, dz \quad (14)$$

(15) The total amount of solids deposited at time $t + \Delta t$ is

$$M_S^t(t + \Delta t) = \sum_{i=1}^n M_S^i(t + \Delta t) \quad (15)$$

(16) The amount of deposited solids per unit area of the pipe clean inner wall is given by

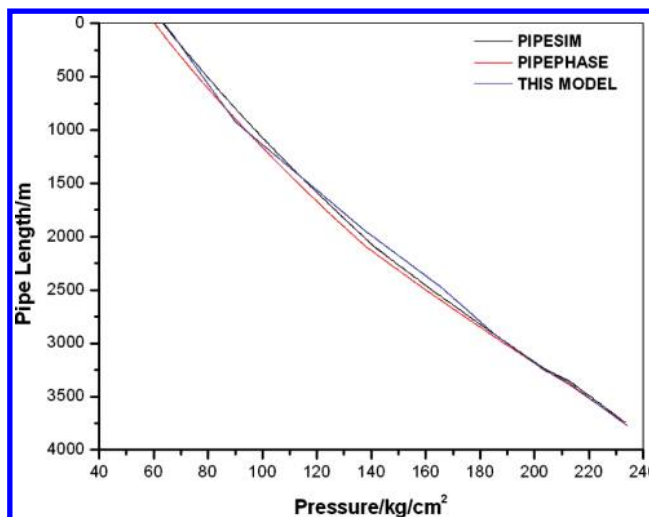$$m_s(t + \Delta t) = \frac{M_S^t(t + \Delta t)}{2\pi R_o L} \quad (16)$$

Figure 7. Pressure gradient match for well B under flowing conditions. Comparison with commercial simulators.
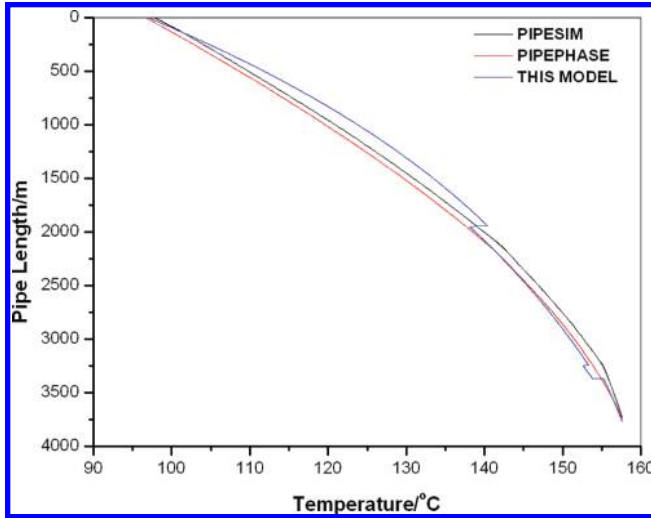
Figure 8. Temperature gradient match for the well B under flowing conditions.

(17) The mass balance for the reference segment follows:

$$(\rho_m Q)_{i+1} = (\rho_m Q)_i - \frac{dM_S^t}{dt} \tag{17}$$

The first term of eq 17 is the fluid mass entering the segment with position $i + 1$ from position i. On the right hand side, the first term stands for the fluid mass exiting position i and the second term is the total deposited mass as a function of time, depending on the particular case considered. If eq 17 holds, then the procedure continues to step 19; otherwise, $p_M^* = p_M \pm \delta$, and it continues to step 9.

(18) The new pipe diameter, which considers the deposited layer, is updated ($D = 2r_w$).

(19) The upper extremes of the intervals $p_2 = p_1 + \Delta P$ and $L_2 = L_1 + \Delta L^{i+1}$ are calculated. If the total length of the pipe is reached, the calculation procedure is concluded; otherwise, we set $p_1 = p_2$ and $L_1 = L_2$ and follow step 2.

4. Sample Calculation

4.1. Well A. The first example involves the study of restrictions caused by asphaltene deposition on the walls of a producing well A, located in Southeast Mexico, creating undesirable plugs that affect flow assurance. Table 1 shows the mechanical configuration of the well. The pipe length is approximately 5300 m. Table 2 shows the measured composition of the live oil produced. Table 3 shows the measured SARA (saturates, aromatics, resins, and asphaltene oil fractions) compositional analysis of the oil stock−tank oil. On the basis of these compositions, and the experimental information on the asphaltene precipitation envelope (APE) of the reservoir fluid, we used the SAFT-VR equation of state (EOS) for fitting the experimentally measured APE. Details of this EOS representation and the thermodynamic assumptions and numerical algorithms involved in this method have been described in detail in the work of Buenrostro-Gonzalez et al.[17] Figure 3 shows the calculated and measured APE's. The EOS result provides a reasonable description of the measured APE. Table 4 presents relevant production data of the particular flow system. Figures 4 and 5 show the calculated pressure−temperature profiles, using the flow model described in Figure 2 (stepwise calculation), with the Mukherjee and Brill[14] correlation for pressure drops.

4.2. Well B. In the second example, we study a real producing well in Southeast Mexico. Table 5 shows the configuration of this so-called directional flowing well. The pipe well length is 3800 m. Figure 6 shows a scheme of the mechanical configuration.

Table 6 presents the measured composition of the reservoir fluid A used in this work, as well as the physical constants of each one of the 43-component mixture. Note that water is present in the system in more than 40% in a mole basis. Table 7 presents all relevant production data of this well, including flow rate, operating pressures and temperatures, water-cut, gas−oil ratio, and other geometrical and mechanical parameters of the flowing system.

The first step in our computational procedure is to match the measured well-head pressure from the knowledge of the bottom hole flowing value at current conditions, using the original cross
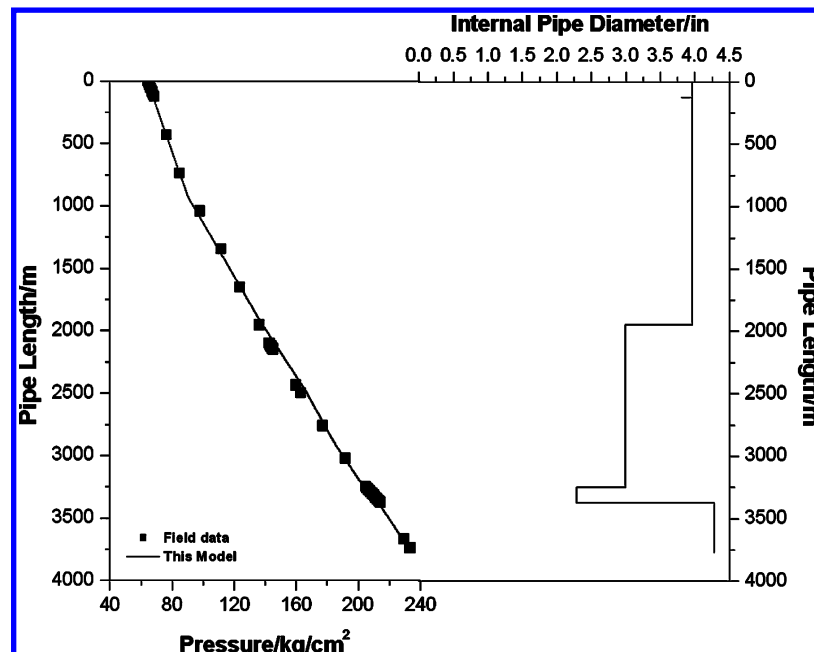

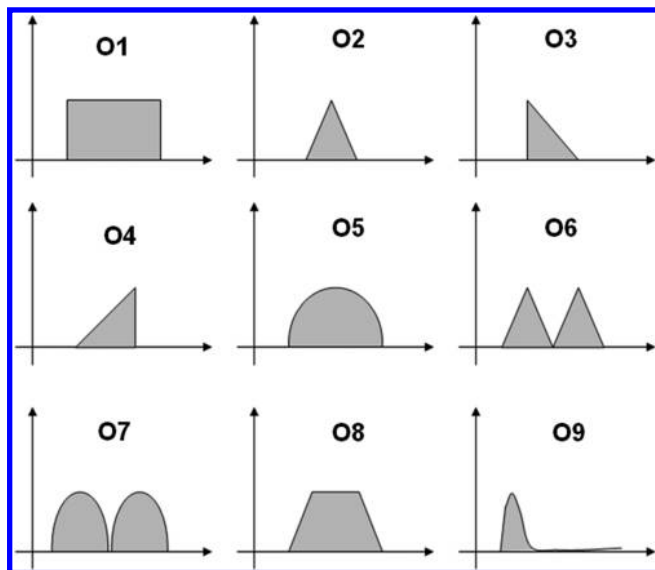**Figure 9.** Mechanical configuration and pressure gradient superposition.

Figure 10. Geometrical restrictions proposed in this study.

Table 8. Geometrical Restrictions in Well B

position	interval/m	length/m
N1	0−126.44	126.44
N2	2007.6−2377.6	370.00
N3	3247.7−3371.4	123.80

section of the well. Figures 7 and 8 show the quality of the match, where, for comparison, results from the PIPESIM 2000[21] (black line) and PIPEPHASE 9.1[22] (red line) commercial simulators have also been plotted. A reasonable agreement among the three calculation methods is evident from these figures.

Figure 9 shows the mechanical configuration of the well, depicting the location of the casing (bottom part) and production sections (upper part) of the whole tubing. Also shown are the results of the pressure-versus-depth matching procedure, where the black squares represent the pressure gradient under flow measured directly in the well. The match is very good. Note that Figure 9 presents the detailed pressure/depth/inner pipe diameter relationship for the well.

Figure 10 shows a total of nine types of geometrical restrictions proposed to study how these affect the total pressure drop profile in the pipeline. Each artificial restriction has three different depths of occurrence (see Table 8) along the well, and
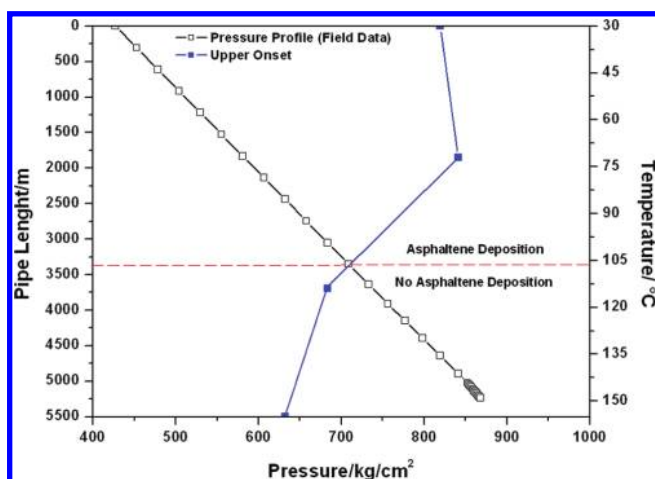

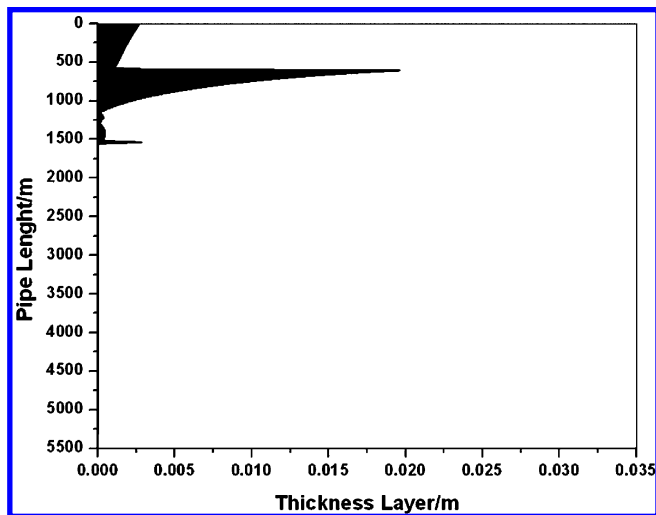Figure 11. Approximate location of asphaltene deposition in well A.

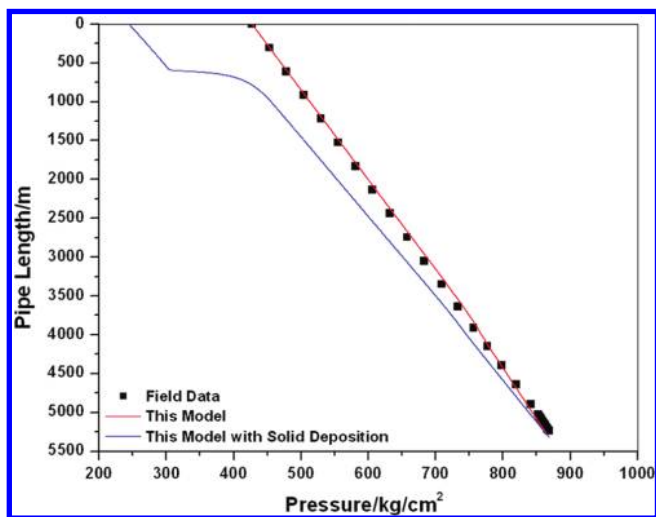Figure 12. Computed asphaltene deposition profile in well A.

Figure 13. Effect of the deposited asphaltenes on predicted pressure gradients.

three different extents of incidence (or "blockage" intensities, i.e. 5, 25, and 50% restriction to the inner pipe diameter available to flow) within the well. The choice of this set of restrictions is rather arbitrary and corresponds to our aim for including different blockage geometries for the production of oil in real wells.

For subsequent discussion, we have labeled the different systems studied with the following notation: ON-DN-N%, where ON refers to the number type of restriction, DN refers to the position of the restriction (according to Table 4), and N% refers to the percent decrease in cross-section diameter. In this way, the notation O1-D1-5% refers to a well having restriction type-1, position 1, and a 5% decrease in the effective diameter, respectively.

Once the pipe and restriction characteristics for all systems were established, we then calculate the corresponding pressure profiles along the pipes, using the computational procedure described in Figure 2, without taking into account the asphaltene deposition.

5. Results and Discussion

5.1. Well A. Figure 11 shows that asphaltene deposition occurs within the production pipeline at the current production conditions, and for a continuous simulation production time of
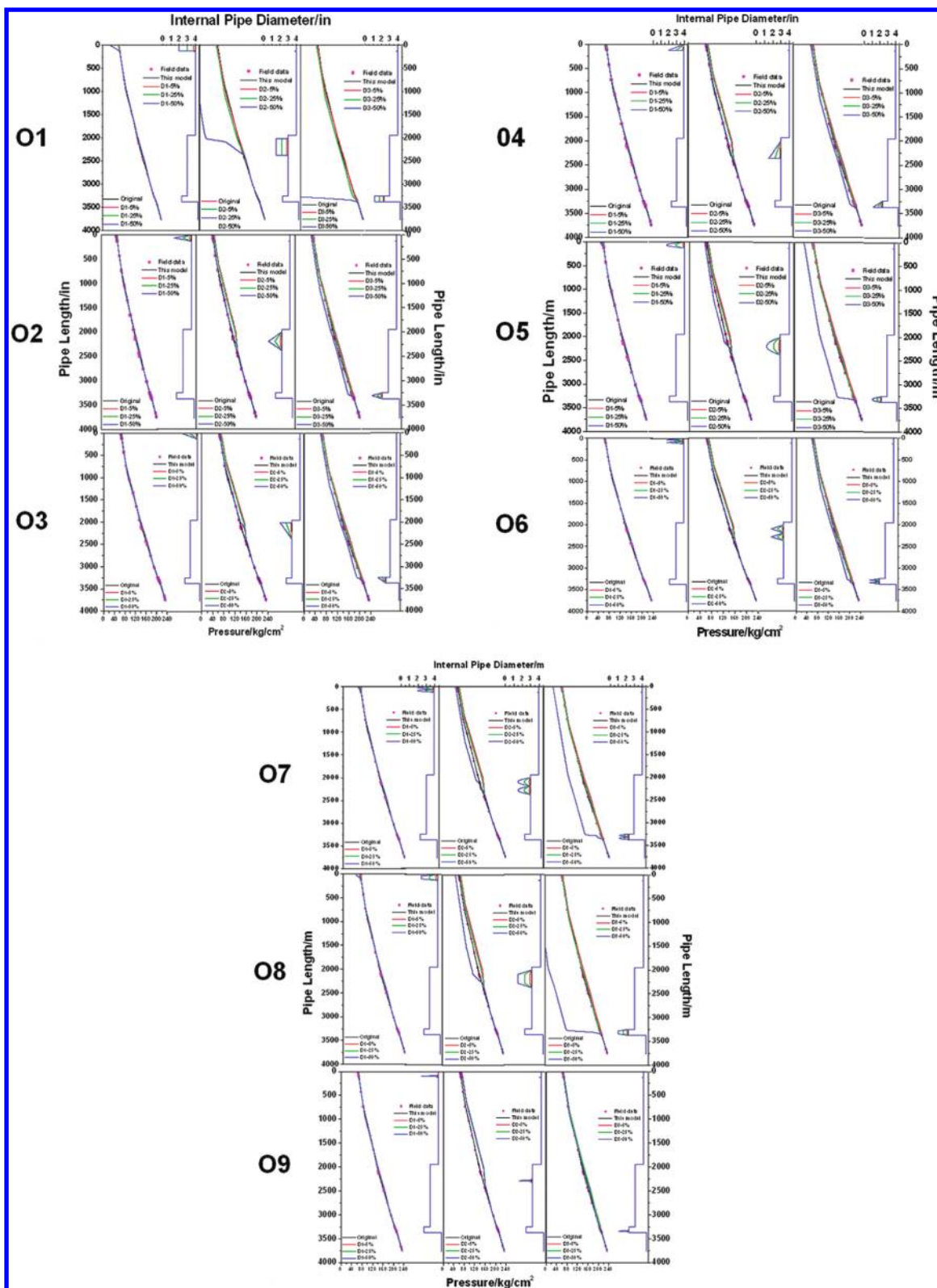
Figure 14. Calculated pressure gradients for restriction types 1−9.

200 days. It is apparent that the model presented in this work predicts the formation of asphaltene plugs within the well starting at a depth of 1550 m, and reaching the wellhead, probably extending along the surface choke, the surface separators and other production facilities. Figure 12 presents the asphaltene deposit profile simulated with this model. In the well, it can be seen that the asphaltene plug geometry has no regular form, but resembles the shape of a nozzle, being the smallest

available diameter to flow located at approximately 750 m downhole, where the diameter reduction is close to 50%.

In Figure 13, the effect that deposited asphaltenes have on predicted pressure profiles under current production conditions is illustrated. It is apparent that the pressure profiles shift to lower values along the production pipe, showing a sharper decrease near the well surface, at a depth of around 750−625 m, which coincides very well with the largest deposit thickness

shown in Figure 12. This reflects a decrease of the computed wellhead pressure to nearly 250 kg/cm², a value 50% lower than the no-asphaltene deposition case.

5.2. Well B. Figure 14 shows the computed pressure-depth profiles, along with the corresponding geometric configuration for all well systems. For instance, systems O1-D1-5% and O1-D1-25% do not alter the pressure profiles significantly, compared to the original (constant diameter) systems. On the contrary, system O1-D1-50% shows that the effect of the O1 type of restriction affects the well capacity to flow significantly, leading to a decrease of up to 58% of the well head pressure (P_{wh}), as compared to its constant-diameter value. For systems O1-D2-5% and O1-D2-25%, the computed pressure profiles do not show a significant alteration, but when a 50% reduction to the diameter available to flow is reached, the well capacity to flow decreases almost in full (the well is only able to produce oil up to a depth of 1250 m, being unable to produce from that depth upward). This phenomenon also affected the wellhead pressure value, which decreased by 98% compared to its original value. For cases O1-D3-5%, 25%, and 50%, no significant effects are observed for the first two restrictions, but for the case of the maximum reduction (50%), the well stops producing at a depth of 3400 m, i.e. the oil barely flows upward some 300 m from the bottom of the well. Again, the wellhead pressure decreases 98% compared to its original value.

For a different restriction, Figure 14 O5 presents the results of the pressure-versus-depth calculation at each one of the three different well depths shown in Table 8. For cases O5-D1-5%, 25%, and 50%, there is no significant variation of the calculated pressure profiles among the three restrictions at this depth (case in O1−O3). Cases O5-D2-5%, 25%, and 50% display an interesting pressure−depth profile along the whole D2 interval shown in Table 8, i.e., at 5% and 25% (red and yellow lines) there is an increase of the calculated pressures as the oil flows up the well, with final P_{wh} increases of 9% and 7% respectively, as compared to the original (constant diameter) values. At the deeper location D3, in Figure 14 O5, it is shown that, again, results at 5% and 25% reduction, reveal an increase in the computed pressures upward the well (P_{wh} increase of 2% and 0.05%, respectively), while, for the maximum reduction (50%), if Figure 14 O5 shows that P_{wh} decreases 47% as compared to its original (constant diameter) value. Other results for different restriction geometries are also shown in Figure 14.

6. Conclusions

We have studied the effect of different restrictions on calculated hydrodynamic parameters of two representative wells from an oil field, one of them, well A, with severe asphaltene deposition problems. The method outlined here takes into account the multicomponent−multiphase nature of the produced hydrocarbons of the wells and combines state-of-the-art hydrodynamic, thermodynamic, and numerical methods to predict the effect of restrictions on well productivity.

From the results obtained, the case of well A shows an asphaltene deposit at above sections of the well after 200 days of simulation. This deposit, with irregular geometry, affects directly the pressure gradient, reducing the wellhead pressure and the oil production of the well. In order to study the effect of the changes in the geometrical configurations of the cross sections at different axial positions, we analyze well B. For this case, the results show that the artificial restrictions affect the calculated pressure profile in different forms and extents; the more influential parameters are the restriction length and thickness. This affects the computed pressure profile from the

mid-depth of the restriction and downstream, where the pressure at the wellhead may decrease significantly. For flow assurance studies, our model provides a reasonable description on the effect that arbitrary restrictions (including those originated from segregated solid phases from an oil, i.e. wax or asphaltene deposition) have on different flow times, well positions, and expected operating conditions. These predictions may be useful in the prevention of production problems related to flow assurance.

Appendix A

Dun and Ros[15] Correlation

In this correlation the variables are the slip velocity (from which the liquid holdup can be calculated) and the friction factor, from which determinations of the flow regime of the oil mixture (i.e., bubble, slug, annular-slug transition, and annular-mist transition) are made. The flow regime is then defined as a function of the dimensionless numbers N_{gv}, N_{Lv}, L_1, L_2, L_S, L_m, and N_d, where

$$L_s = 50 + 36 N_{Lv}$$
$$L_m = 75 + 84 N_{Lv}^{0.75}$$
$$N_{LV} = v_{sL} \sqrt[4]{\frac{\rho_L}{g_c \sigma_L}} \tag{A1}$$
$$N_{gV} = v_{sg} \sqrt[4]{\frac{\rho_L}{g_c \sigma_L}}$$

Here, ρ_L is the liquid density (oil and water, if this is in the mixture), σ_L is the liquid−gas surface tension, d is the inner pipe diameter, g_c is the gravitational conversion constant, v_{sL} and v_{sg} are the surface liquid and gas velocities. L_1 and L_2 are functions of the dimensionless number N_d which is defined as

$$N_d = 120.872 d \sqrt{\frac{\rho_L}{\sigma_L}} \tag{A2}$$

These authors also developed correlations for the dimensionless slip velocity, S, from which the actual slip velocity, v_s and liquid holdup, H_L, can be calculated according to the following equations

$$v_s = v_g - v_L = \frac{v_{sg}}{1 - H_L} - \frac{v_{sL}}{H_L} \tag{A3}$$

and

$$H_L = \frac{v_s - v_m + [(v_m - v_s)^2 + 4 v_s v_{sL}]^{0.5}}{2 v_s} \tag{A4}$$

The pressure drop contribution due to elevation can be calculated according to the following expression,

$$\left(\frac{dP}{dz}\right)_{el} = \frac{g}{g_c} \rho_s \tag{A5}$$

In eq A5, ρ_s refers to the mixture density considering slip between phases

$$\rho_s = \rho_L H_L + \rho_g(1 - H_L) \tag{A6}$$

The friction contribution to pressure drop is calculated depending on the flow regime occurring in any given pipe length according to the following limits:

Bubble Flow ($0 \le N_{gv} \le L_1 + L_2 N_{Lv}$).

$$\left(\frac{dP}{dz}\right)_f = \frac{f_m \rho_L v_{sL} v_m}{2 g_c d} \tag{A7}$$

Slug Flow ($L_1 + L_2 N_{Lv} \le N_{gv} \le L_s$). In this case, the pressure drop is calculated using the same expression as in bubble flow.

Mist Flow ($N_{gv} > L_m$).

$$\left(\frac{dP}{dz}\right)_f = \frac{f \rho_g v_s v_{sg}^2}{2 g_c d} \tag{A8}$$

The pressure drop due to acceleration is given by

$$\left(\frac{dP}{dz}\right)_{acc} = \frac{v_m v_{sg} \rho_n}{g_c P} \frac{dP}{dz} \tag{A9}$$

where ρ_n is the no-slip mixture density, P is the pressure, v_m and v_{sg} are the mixture and gas velocities.

Transition Flow ($L_s < N_{gv} < L_m$). For the transition zone between slug and mist flow regimes, Dun and Ros[15] suggested a linear interpolation between parameters L_s and L_m. The calculation of the pressure gradient due to friction involves expressions corresponding to each flow regime. The expression used to compute the gradient is

$$\left(\frac{dP}{dz}\right)_{transition} = A\left(\frac{dP}{dz}\right)_{slug} + B\left(\frac{dP}{dz}\right)_{mist} \tag{A10}$$

where

$$A = \frac{L_m - N_{gv}}{L_m - L_s}$$
$$B = \frac{N_{gv} - L_s}{L_m - L_s} = 1 - A \tag{A11}$$

Finally, the total pressure drop for the segment dz is then calculated according to

$$\left(\frac{dP}{dz}\right)_{Tot} = \frac{\left(\frac{dP}{dz}\right)_{el} + \left(\frac{dP}{dz}\right)_{fr}}{1 - E_k} \tag{A12}$$

where

$$E_k = \frac{v_m v_{sg} \rho_n}{g_c P} \tag{A13}$$

Mukherjee and Brill[14] Correlation

This correlation fits adequately data of the dynamic pressure gradient versus well depth. The empirical equations that define the flow maps for the different flow regimes are (subindex BP, PAM, and ST refer to bubble-plug, plug-annular-mist, and stratified, respectively) the following:

$$N_{Lv_{BP}} = 10^X \tag{A14}$$

where

$$x = \log N_{gv} + 0.940 + 0.074 \sin \theta - 0.855 \sin^2 \theta + 3.695 N_L \tag{A15}$$

An increase in the liquid viscosity speeds up the plug-annular-mist transition, according to

$$N_{gv_{PAM}} = 10^{(1.401 - 2.694 N_L + 0.521 N_{Lv}^{0.329})} \tag{A16}$$

In descending and horizontal flow, the bubble-plug transition is given by

$$N_{gv_{BP}} = 10^y \tag{A17}$$

where

$$y = 0.431 - 3.003 N_L - 1.138(\log N_{Lv})\sin \theta - 0.429(\log N_{Lv})^2 \sin \theta + 1.132 \sin \theta \tag{A18}$$

This transition generates a family of curves for different inclination angles and liquid viscosities. The total pressure drop calculation is defined as

$$\left(\frac{dP}{dz}\right)_{Tot} = \frac{\frac{f \rho_S v_m^2}{2d} + \rho_S g \sin \theta}{1 - E_K} \tag{A19}$$

where f is the factor friction, ρ_s is the mixture density considering slip between phases, d is the inner pipe diameter, v_m is the mixture velocity, θ is the angle form the horizontal, and

$$E_K = \frac{\rho_s v_m v_{sg}}{P} \tag{A20}$$

Notation

API = specific gravity
d = diameter, in,
D_{in} = internal pipe diameter, in.
f_m = friction factor
g_c = gravitational conversion constant ($= 32.2$ lb$_m$·ft/lb$_f$·s^2)
H_L = liquid holdup
L_m = dimensionless function
L_S = dimensionless function
L_1 = dimensionless function
L_2 = dimensionless function
MW = molecular weight
N_{gv} = gas velocity number
N_{Lv} = liquid velocity number
N_d = pipe diameter number
P = pressure, psia
P_b = bubble point pressure, psia
P_c = critical pressure, psia
P_{wf} = well bottoms flowing pressure, psia
P_{wh} = wellhead flowing pressure, psia
Q_L = volumetric flow rate of liquid, STBW/D
Q_o = volumetric flow rate of oil, STBO/D
GOR = gas−oil ratio, ft^3/STB
T_b = normal boiling temperature, °C
T_c = critical temperature, °C
T_{wf} = well bottoms flowing temperature, °C
T_{wh} = wellhead flowing temperature, °C
TP = production tubing
U = overall heat transfer coefficient, BTU/ft^2·h·°F
V_c = critical volume, STB/lb-mol
V_g = actual gas velocity, ft/s

V_L = actual liquid velocity, ft/s

V_m = actual mixture velocity, ft/s

V_s = slip velocity, ft/s

V_{sg} = superficial gas velocity, ft/s

V_{sL} = superficial liquid velocity, ft/s

Z_i = composition of component i

Greek Letters

ρ_s = slip density, lb_m/ft^3

ρ_L = liquid density, lb_m/ft^3

ρ_g = gas density, lb_m/ft^3

ϕ = function in eq 9

ΔL = pipe length section, m

ω_i = acentric factor of component i

θ = inclination angle of a pipe

Literature Cited

(1) Neusen, K. F. *Optimizing of flow parameters for the expansion of very low-quality steam*, Report UCRL-6152; Lawrence Radiation Laboratory, University of California, Livermore, CA, 1962.

(2) Maneely, D. J. *A study of the expansion process of low quality steam through a de Laval nozzle*, Report UCRL-6230; Lawrence Radiation Laboratory, University of California, Livermore, CA, 1962.

(3) Brown, R A. *Flashing expansion of water through a converging-diverging nozzle*, Report UCRL-6665-T; Lawrence Radiation Laboratory, University of California, Livermore, CA, 1961.

(4) Fiedler, R. *A Shock location during two-phase flow in an over-expended nozzle*, Report UCRL-6676; Lawrenoe Radiation Laboratory, University of California, Livermore, CA, 1961.

(5) Vogrin, J. *An experimental investigation of two-phase two-component flow in a horizontal, converging-diverging nozzle*, Report ANL-6754; Argonne National Laboratory, Argonne, Illinois, 1963.

(6) Hesson, J. C.; Peck., R. E. Flow of two-phase CO_2 through orifices. *AIChE J.* **1958**, *4*, 207–210.

(7) Petrick, M. *Two-phase air-water flow phenomena*, Repot ANL-5787; Argonne National Laboratory, Argonne, Illinois, 1958.

(8) Straub, L. G.; Silverman, E. *Air-water mixture flow through orifices, bends, and others fittings in a horizontal pipe*, Report No. 63; St. Anthony Falls Hydraulic Laboratory, University of Minnesota, 1960.

(9) Janssen, E.; Kervinen, J. A. *Two-phase pressure drop across contractions and expansions of water-steam mixture at 600 to 1400 psia*, Report Geap 4622-1965-US; 1966.

(10) Aloui, F.; Souhar., M. Experimental study of a two-phase bubbly flow in a flat duct symmetric sudden expansion--part 1: visualization, pressure and void fraction. *lnt. J. Multiphase Flow* **1996**, *22* (4), 651–665.

(11) Ahmed, W. H.; Ching, C. Y.; Shoukri., M. Pressure recovery of two-phase flow across sudden expansions. *Int. J. Multiphase Flow* **2007**, *33*, 575–594.

(12) Chen, I. Y.; Tseng, C.-Y.; Lin, Y.-T.; Wang, C.-C. Two-phase flow pressure change subject to sudden contraction in small rectangular channels. *Int. J. Multiphase Flow* **2009**, *35*, 297–306.

(13) Ramírez-Jaramillo, E.; Lira-Galeana, C.; Manero., O. Modeling Asphaltene Deposition in Production Pipelines. *Energy Fuels* **2006**, *20*, 1184–1196.

(14) Mukherjee, H.; Brill, J. P. Liquid Holdup Correlations for Inclined Two-Phase Flow. *JPT* **1983**, 1003–1008.

(15) Dun, H.; Ros, N. C. J. Vertical flow of gas and liquid mixtures in wells. *Proceedings of the 6th World Petroleum Congress*, 1963; p 451.

(16) Peng, D. Y.; Robinson, D. B. A New-Constant Equation of State. *Ind Eng. Chem.* **1976**, *15* (1), 59–64.

(17) Buenrostro-Gonzalez, E.; Lira-Galeana, C.; Gil-Villegas, A.; Wu. Asphaltene Precipitation in Crude Oils: Theory and Experiments. *AIChE J.* **2004**, *50*, 2552–2570.

(18) Romero-Juarez, A. A Simplified Method for Calculating Temperature Changes in Deep Wells. *JPT*, **1979** (June).

(19) Svendsen, J. A. Mathematical Modeling of Wax Deposition in Oil Pipeline Systems. *AIChE J.* **1993**, *39*, 1377–1388.

(20) Kern, D. Q.; Seaton, R. E. A Theoretical Analysis of Thermal Surface Fouling. *Brit. Chem. Eng* **1959**, *4*, 258.

(21) *PIPESIM Electronic manual*; Schlumberger, 2003.

(22) *PIPEPHASE V.9.1, Electronic manual*; Invensys Precess Systems, 2008.